

GEOFYSICS :

Reconstruction of the Earth Model and Discovery of the Interior Dark Matter

HSIEN-JUNG HO

Newidea Research Center

Website: <http://newidea.org.tw>

E-mail : newidea.ufoho@msa.hinet.net

10 Fl, No. 110-6, Jie-Shou N Road, Changhua, 50060 Taiwan.

Abstract

Based on the recommendations of several geophysicists and a confirmed topography of the core-mantle boundary more than 10 km height, a new earth model has been developed. According to this model, the chemical composition between the lower mantle and the outer core, are like each other and the density distributions of both are continuous at the core-mantle boundary. As a result of the study, we can infer that the solid rock in the lower mantle and the liquid molten rock or magma in the outer core change states interactively. In the F transition zone of the outer core, some elements and the components undergo oxidation-reduction reactions with each other and separate because of gravity. The abundant iron oxides in the outer core are partially reduced to iron, which alloys with certain amounts of nickel and combines with a great number of oxides to settle down in the inner core and solidify. The great amount of the heat produced due to the chemical reaction in the F zone and solidification at the inner core boundary becomes the geodynamic of a large convection cell, a circulation of magma and solid or molten rock migrating up to the crust and down to the F zone. Using a simplification method to calculate the data of the new earth model, the earth's mass and moment of inertia are found only to be 5121.82×10^{24} g and 76126.841×10^{40} g.cm². The physics conceptions of dark matter and sing theory are introduced to solve the problems of the missing mass and the insufficiency of moment of inertia. Finally, a dark planet inside the earth has been figured out, which has a radius of 3700.375 km and a mass of 852.38×10^{24} g about 1.33 times that of Mars.

Key Words: Earth model, Density jump, Convection cell, Chandler wobble, Darkmatter, Solar-neutrino, Ten-dimensional theory.

I . Introduction

When stars at the outside edge of a galaxy are orbiting at high speed, the total mass of the galaxy, whose gravity keeps stars from escaping, can be estimated from the mass of the stars and its speed of rotation. The total mass of stars in a galaxy, which can be estimated by observing the galaxy with an astronomical telescope, is less than 10% of this total mass of the galaxy estimated from the orbiting stars. The phenomenon appears throughout the universe. Unobservable matter, amounted to more than 90 % mass of the entire universe, is called dark matter, which can only be detected by its gravitational influence on visible matter. All astronomers agree on the existence of dark matter, however, after a twenty-year search, they have not found any evidence of it. So, dark matter, the densest matter in the universe, is a major problem, which still has no solution. The best approach to dark matter research is to begin with the planet on which we live.

In the current earth model utilized in seismological investigations, such as body-wave travel times, surface-wave dispersion, and free oscillation periods for researching the chemical composition and the density distribution of the earth, the portions of the crust and the upper mantle have been analyzed with satisfactory accuracy. Regarding the lower mantle and the core portion, however, there remain number questions to be answered. The mantle and the core are not in chemical equilibrium and the fine structure of the core-mantle boundary (CMB) is not well understood. Although some hypotheses such as the existence of a D" transition zone in the lower mantle and iron combined with oxygen as the primary alloying constituent are suggested and a lot of advances of this research have come out, but there are also some discrepancies in the interior of the earth [Creager & Jordan, 1986; Morelli & Dziewonski, 1987]. Furthermore, there is no conclusive evidence that the inner core is in thermodynamic equilibrium with the outer core. The main problem is a lack of phase equilibrium data for plausible core compositions at the appropriate conditions, added to the fact that seismological observations do not yet offer a decisive constraint on the difference in composition between the inner and outer core [Jangles, 1990]. Based on the found conceptions in the deep interior, some reconstructed new earth models should be figured out by applying geophysics to reasonably analyze the interior constitution, composition, temperature and pressure of the earth. According to the trial curves of density distribution of the new earth models, the earth's mass and moment of inertia are calculated from it by a simplification method to match the real earth's figure. The differences in quantity between the actual observed values and the values calculated from these trial curves are the missing values of the mass and the moment of inertia of the earth. These missing values belong to dark matter in view of the astrophysics.

Based on contemporary physics — Superstring Theory, which has the characteristics of ten-dimensional space-time and the Super symmetry of $E_8 \times E_8$, the radius and the density of dark matter should be calculated from a combination of gravitational influences of the earth and the missing mass through geophysics. Finally, the combined data of the earth and dark matter are compared with that of the Preliminary Reference Earth Model (PREM) [Dziewonski & Anderson, 1981] to theoretically confirm whether a dark planet exists.

II . The Interior Constitution of the Earth

About the earth's interior, the constitution of the deep interior is uncertain with some difficulties. To conduct further investigation, the PREM is taken as the current earth model in this paper (fig.1).

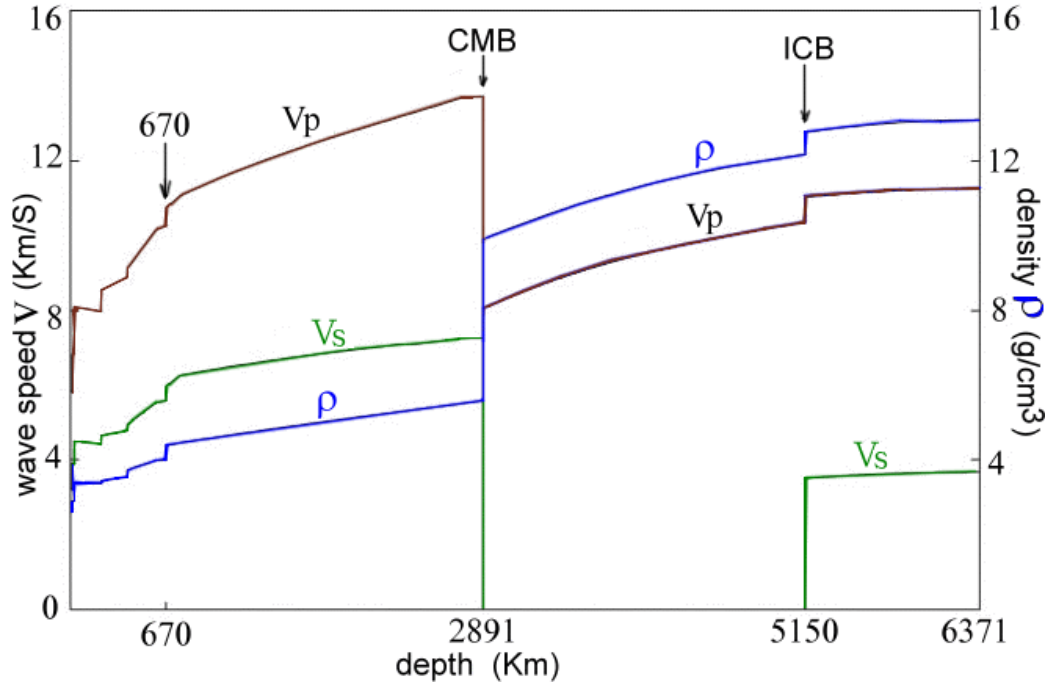


Fig. 1 The data of PREM : ρ : density ; V : velocity.

At the CMB of this model, the solid portion of the lowermost mantle has a density of 5.57 g/cm^3 , which jumps to 9.90 g/cm^3 in the liquid portion of the top core, a jump of 77.74 %. According to the physiochemical data, the average density of solid matter decreases by about 10 % when it melts into liquid state in the atmosphere, however, in the PREM the density jumps significantly at the CMB. All investigations cannot confirm the data directly. So, research about the interior constitution of the earth is needed, especially at the CMB. There are two chief factors relating to the large density jump at the CMB:

A. Elastic mechanics guides the relative equations of seismic body wave velocity and density:

$$V_p = [(\lambda + 2\mu) / \rho]^{1/2} \quad (1)$$

$$V_s = (\mu / \rho)^{1/2} \quad (2)$$

And the Adams-Williamson equation:

$$d\rho/dR = -GMP/R^2 [V_p^2 - (4/3) V_s^2] \quad (3)$$

The outer part of the core is in a liquid state. Below the CMB, V_p suddenly drops to a very low velocity and V_s and μ both drop to 0. So, from the first two equations below the CMB the density will jump highly. Since the gravity of the earth places considerable pressure on the core, the resultant pressure exceeds the elasticity range of molten rock or magma; therefore, the first two equations are not suitable for evaluating the core density. Bullen used equation (3) to investigate the moment of inertia of the core alone and found it ($0.57Mr^2$) to exceed that of a uniform sphere ($0.4Mr^2$) [Bullen, 1940]. So, equation (3) was rejected. Then Birch added a term ($-\alpha\rho\tau$) to the right of the equation to revise it [Birch, 1952], however, the discontinuity in density at the core boundary cannot be determined directly from the revised equation. In addition, the

two soft layers in the upper part of the mantle are generally consistent with low wave velocity regions. Solomon proposed that the low wave velocity region, partial melted region, is due to small amounts of liquid between granules [Solomon, 1972]. The density of the soft layer will not increase sharply by decreasing the velocity of seismic waves. For the same reason, wave velocity decreasing below the CMB is due to the liquid state of the outer core, a physical phenomenon of the liquid state, and is not due to a large density jump.

B. Based on the known values of the earth's mass and moment of inertia, there are the great amounts of rest values deducting the certain quantities of the portion in the crust and in the mantle. In order to match it, the ordinary way is to set a high-density distribution in the core and also a high density jumps at the CMB. It is unnecessary to consider the first factor, but the second one is considered as a matter of course within the domain of current science. If the second factor is not initially taken into consideration, a different conclusion should be drawn from the four statements in the topic of the CMB as follows.

1. Ramsey and Lyttleton have challenged the concept of an iron core, suggesting that under high temperature and pressure at the CMB the mantle silicates undergo phase changes, a solid phase changing into a liquid phase in the top core, to produce the material of high density, low melting point and electrical conductivity. Ramsey's hypothesis is still accepted by a few geophysicists for several reasons [Ramsey, 1948; Lyttleton, 1973].

2. Knopoff showed that across a phase transition near the surface, one can predict that the bulk modulus K increases by the increasing of the density ρ ; in such a way, the ratio $K / (\rho^{7/3})$ keeps constant. From the models, the bulk modulus remains unchanged across the CMB. It is difficult to account for a large density jump from about 5.57 g/cm^3 to about 9.90 g/cm^3 . On this basis, it is difficult to argue in favor of the density distribution to be smoothly continuous at the CMB and a core of silicate composition [Knopoff, 1965].

3. Buchbinder studied the variation in amplitude, with distance Δ , of the reflected phase PcP. He found that the amplitude-distance curve, which displays a minimum at $\Delta = 32^\circ$, was not consistent with the computed reflection amplitudes for a solid liquid interface if the previously accepted values of V_p and density were employed. A model proposed by Buchbinder, which is consistent with the observed amplitudes, provides no discontinuity in density between the low mantle and the core. Such a model may arise if there is considerable mixing of the core material with the lowermost mantle, and vice versa [Buchbinder, 1968].

4. A topography of the core-mantle boundary, determined from the arrival times of reflected and transmitted waves shows the results of an inversion indicating more than 10 km of relief with $3000 \sim 6000 \text{ km}$ scale lengths [Morelli & Dziewonski, 1987].

The depressed regions of the topography are dynamically supported by down welling of cool mantle material [Gudmundsson *et al.*, 1986; Lay, 1989]. Approximately 80 % of the hot spots at the earth's surface are manifestations of plumes rooted in the deepest part of the mantle near the CMB. In three-dimensional maps of the earth's interior the topography of the core, different from that predicted by the hydrostatic equilibrium theory, contains information important to geodynamic processes and the geomagnetic secular variation.

Topography on the CMB is likely to result from convection in the overlying mantle [Young & Lay, 1987]. But some agreements of that are determined by processes in the core [Bloxxham & Jackson, 1990]. This relief

is dynamically supported and provides coupling between the mantle and the core. It has been well known that there are two convections circulated individually below the crust to the lower mantle and in the outer core. Ruff and Anderson argue for dynamo action in the core maintained by differential heating of the core by the mantle [Ruff & Anderson, 1980]. Bloxham and Gubbins argue that flow near the core surface may be controlled by lateral temperature variations in the lowermost mantle, which are amply sufficient for this to be a significant effect [Bloxham & Gubbins, 1987]. But the lateral temperature variations near the outer core surface are exceedingly small, amounting to only a few mills Kelvin, based on $\alpha = 5 \times 10^{-6} \text{K}^{-1}$ [Stevenson, 1987]. The lateral temperature variations in the lowermost mantle are so small that it should not affect the flow near the core surface. Studying the dynamics of the liquid core, the lateral heterogeneities below the detectable level associated with density differences $|\delta\rho/\rho| > 10^{-5}$ is supported, i.e. lateral homogeneity of the liquid core [Morelli & Dziewonski, 1987] (Fig. 2).

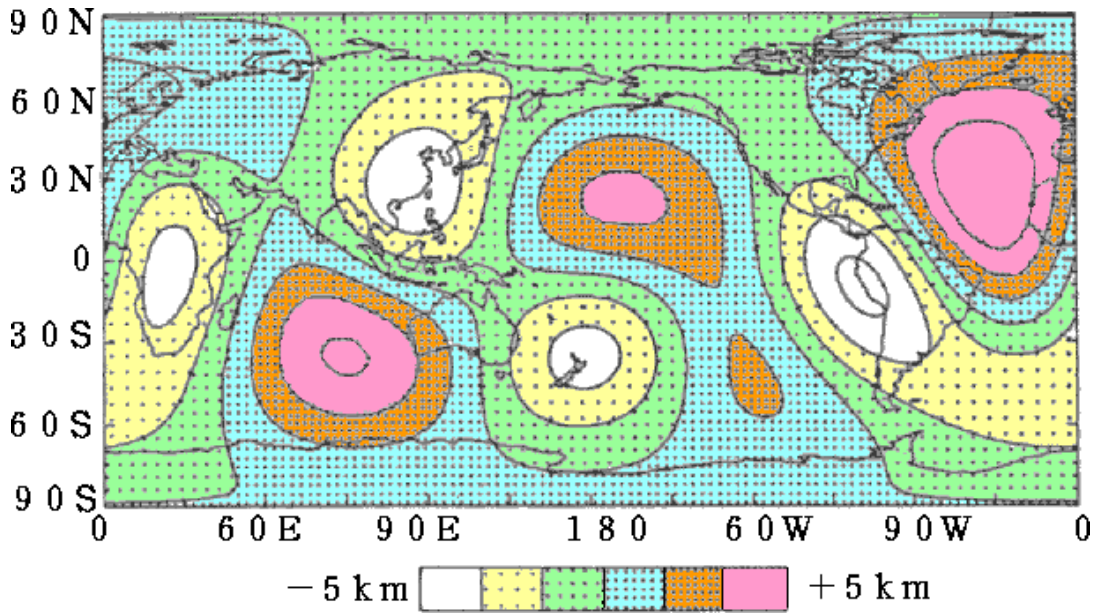


Fig. 2 Topography of CMB obtained by inversion of the combined PcP and PkP_{BC} data set (Morelli & Dziewonski)

The lateral density differences in the top of outer core are so small that it could not provide a relief in excess of 10 km at the CMB. According to the PREM, there is a density jump of 4.33 g/cm^3 at the CMB. Neglecting the gravity anomaly, the lateral difference in pressure at the lowermost level of the CMB is 4.246 kbar considering a height of only 10 km. This pressure should reduce an increasing iron density of $6.323 \times 10^{-3} \text{ g/cm}^3$ under condition at the top of core, yielding a density difference of $\delta\rho/\rho = 0.639 \times 10^{-3}$, which is far beyond 10^{-5} supported by Morelli and Dziewonski [Morelli & Dziewonski, 1987].

Since the D'' transition zone, where sustains the chemical and the thermal equilibriums between the mantle and the core, is rejected and the density differences are smaller than 10^{-8} , there is a significant suggestion that the density difference between the liquid state and solid state at the CMB must be very small or nearly equal, i.e. the hypothesis that the similar materials of a solid and a liquid change state each other at the CMB to produce the core topography. Thus, based on the topography, the idea of a spherical structure of the CMB has been challenged, so a new study is necessary to determine the actual model.

Considering the previous statements that the slopes of the density curve are continuous between the lower mantle and the outer core, and the states of solid and liquid interactively change with each other at the CMB, topography may have a mechanical rather than thermal effect on the flow [Gubbins & Richards, 1986]. On this basis, it is obviously in terms of the geodynamic processes that only the vertical interactions of material and the temperature between the lower mantle and the outer core are the main cause. Based on this view to find the truth, we could figure out a reasonable way that the migrating masses of rock or molten rock sink downward and magma up well in plume rises upward in a great convection cell from the F transition zone of the outer core to the crust. The flow of convection penetrates through the CMB and that should affect the topography of the core. These inferences indicate that material of the outer core mixes with that of the lower mantle, dominantly silicates. Therefore, the PREM, in which the density curve jumps by 77.74 % at the CMB, should be an unreasonable basis of inference.

At the inner-outer core boundary (ICB), a density jumps of about 1.8 g/cm^3 was calculated by Bolt and Qamar [Bolt & Qamar, 1970]. Bolt clearly observed both low angle and steep incident reflections PKiKP of about one second period at the ICB. The mean amplitude ratio PKiKP/PcP suggests a density jump of 1.4 g/cm^3 there [Bolt, 1972]. Recently the density contrast at the ICB has been deduced from the amplitude ratio PKiKP/PcP, and the density jump of $1.35\text{--}1.66 \text{ g/cm}^3$ there has been obtained for a quality factor in the outer core higher than 10,000 [Souriau & Souriau, 1989]. At the ICB, a density jumps of 0.59 g/cm^3 in the PREM is too small to compare with the previous data.

From this information, the density jump between the lighter liquid outer core and the solid inner core seems to be too large to represent a simple volume change on condensing as the same components change from a liquid state into a solid state. The composition of the outer core is not likely to be the same as that of the inner core, since a liquid in equilibrium with a solid phase in a multi-component system does not have the same composition as the solid [Hall & Murthy, 1972]. In order to confirm a reasonable constitution of the earth, the chemical composition of the core must be further investigated.

III. The chemical composition of the core

The composition of the earth's core is one of the most important and elusive problems in geophysics. From the necessity of the seismic wave velocities, cosmic chemical abundances and the geomagnetic requirements, the current model of the core is one almost filled with molten iron. Several geophysicists suggest that the main component of the outer core is iron combined with a small amount of a light element such as sulfur or oxygen. Ringwood proposed that oxygen, rather than sulfur, is the major alloyed light element incorporating with FeO in the outer core [Ringwood, 1977]. However, there is no perfect explanation of any lighter element, which satisfies the apparent chemical equilibrium between the core and the mantle.

In three-dimensional maps, tomographic models represent an instantaneous, low-resolution image of a convecting system. Detailed interpretation knowledge of mineral and rock properties that are, as yet, poorly known is required. A complex set of constraints on the possible modes of convection in the earth's interior has not yet been worked out; this will require numerical modeling of convection in three dimensions.

Thus, the interpretation of the geographical information from seismology in terms of geodynamical processes is a matter of considerable complexity [Woodhouse & Dziewonski, 1989]. The topography on the CMB can be sustained only by dynamic processes, and these processes must be crucially understood.

According to the inference above, the main components of the lower mantle and the outer core are similar. The main component of the outer core is not liquid iron alloying with iron oxides, but silicates, similar to the main component of the lower mantle. Based on mineralogy, the main mineral of the mantle is pyrolite, a compound of silicates, and the main component of the outer core is also pyrolite but only in a liquid state. Under the same conditions, the higher the temperature under which common minerals are produced, the lower the polymerization is and vice versa. The closer the crystal minerals of the mantle under the temperature and pressure are to the core, the more the polymerization losses of crystalline mineral. Then the bonding force of mineral compound is destroyed, and the crystallization gradually diminishes.

Olivine, an important rock of the earth, for example, under room temperature and pressure is a complex crystal tectosilicate. Quartz is a mineral of Olivine. After heating, quartz, the four oxygen of the silicon oxygen tetrahedron and four different structures of silicon oxygen tetrahedron are gradually reduced to phyllosilicates, inosilicates and cyclosilicates, respectively. When the temperature raises considerably high, the four oxygen of silicon oxygen tetrahedron become an elemental unit of silicates known as sorosilicates. When the temperature reaches the melting point, the sorosilicates reduce to nesosilicates, which are the crystal tetrahedron of silica mineral, a basic structural unit of minerals.

At the CMB, the temperature is $4500 \pm 500^\circ\text{K}$ that reaches the melting point of rock under that pressure. In the F zone of the deeper core, $5500 \sim 6600^\circ\text{K}$, polymerization may cease completely, and mostly bonding power of ions loses, only the electronic bonding force exists. All the ions and molecules may become unbounded. Therefore, the molten rock becomes magma, a mixture of oxides such as SiO_2 , Al_2O_3 , FeO , Fe_2O_3 , Cr_2O_3 , MgO , NiO , etc., and metals, such as Fe, Ni, Mn, etc.

In the higher resolution models, some of the heterogeneities extend upward from the CMB into the mantle in a manner suggestive of rising plume structure [Young & Lay, 1987]. On this basis, a great quantity of magma heated by the extreme temperatures in the core condenses into solid rock and produces the heat of solidification at the CMB. Some magma absorbing that heat does not condense but mixes with masses of rock as honeycombed blobs of rock rising upward at approximately an inch a year through the mantle to pour out at cracks in the mid-ocean ridge to form new ocean floor or in the continent to form great rifts. The outflow of heat is the dynamic source of continental drift. Conversely, due to convection, the downward migrating masses of cold rock in the subduction zone of the crust sink all the way through the warmer surrounding mantle to the CMB. The downward masses of rock in the cold regions of the low mantle produce depressions of the CMB into the core, and both the cold region in the mantle and a depression of the CMB produce downwelling flow in the core [Bloxham & Jackson, 1990].

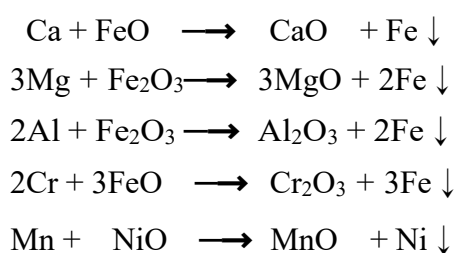
The energy source and buoyancy sources in the core are still not well understood, but we attempt to explain this phenomenon from the perspective of the great convection cell as described above. The downward masses of rock absorb the heat of fusion, diminishing the heat energy at the CMB, and melting in the core, where viscosity is so high that the great quantities of molten rock cannot diffuse but still remain

a whole. So, the components of molten rock are seldom involved in the chemical reactions.

According to mechanics, although the velocity of downward migrating flow is low, the mass of the rock column from the crust to the CMB is so large that its downward momentum has a great quantity. In the liquid outer core, there is no rigid body having enough mass to counteract the downward momentum, so the molten rock sinks all the way to the inner core. The great downward momentum is counteracted by the solid inner core, which Jeanloz and Wenk have obtained evidence of low-degree convection like that in the mantle in the inner core from an enigmatic observation [Jeanloz & Wenk, 1988]. At the ICB, the momentum from the downward molten rock is transmitted through the core, the earth's center and on to the opposite side of the CMB.

From ray theory, an evidence of reduced velocity gradient in a zone above the inner core boundary has been interpreted [Rial & Cormier, 1980; Cormier, 1981]. A higher resolution solution for the core velocity and wave amplitudes by A. Qamar confirms the F transition zone, 566 km in width, above the ICB [Bolt, 1972]. At the boundary of the transition zone F, where the velocity of body wave jumps about 0.1 km/sec, the viscosity of molten rock has been reduced, and the molten rock is able to flow more freely and became a heterogeneous mixture —magma. Oxides and metals, the component of magma, could diffuse freely and float or sink according to their specific gravity. We suggest that the F zone should have some functions instead that of the well-known D" zone, such as the thermal and chemical equilibrium.

There is a large amount of iron oxides (FeO, Fe₂O₃) in the mantle, and the deeper the mantle is the higher the proportion of iron oxides. Altshuler and Sharipdzhanov proposed that an iron oxide which has metal-like density and electrical properties at high pressures and temperatures exists in the earth's core would be a compromise between extreme views of the metallic phase and in conformity with the high cosmic abundance of oxygen [Altshuler & Sharipdzhanov, 1971]. From this information, we propose that the outer core would be rich in iron oxides. Bloxham and Gubbins inferred that topography and lateral temperature variations in the lowermost mantle have an indistinguishable effect on the magnetic field. In view of the topography, the downward migrating magma rich in iron oxides is affected by diffusion, obstruction of the inner core, tangentially geostrophic flow, and toroidal flow, so the fluid flows westward, which causes the geomagnetic secular variation [Bloxham & Gubbins, 1987]. So, under low viscosity, the oxides and metals can flow vertically and horizontally, thus allowing mutual oxidation-reduction reactions to take place easily in the F region. The active light metals take oxygen from heavy metal oxides and are further oxidized into light metal oxides. The heavy metal oxides are reduced to heavy metals and sink. For example:



CaO, MgO, Al₂O₃, Cr₂O₃ and MnO float in the F zone, and FeO, Fe₂O₃ and NiO become iron and nickel, which sink down to be the main component of the inner core. These oxidation-reduction reactions are exothermic processes that produce a great amount of heat. The reduced iron alloys with certain amounts of nickel and combines with oxides to settle down at the ICB and produces the heat of solidification while it solidifies. In the F zone, magma diffuses and absorbs a great amount of heat to rise to the CMB and condenses into solid rock as the beginning of the process of large convection cell starts anew. The great amount of heat, produced from the chemical reaction and the solidification at the ICB and the CMB and from the fusion heat lost at CMB while the down welling rock melts, causes the power sources for the geodynamo of a large convection cell. A schematic diagram of this scenario is shown in Figure 3.

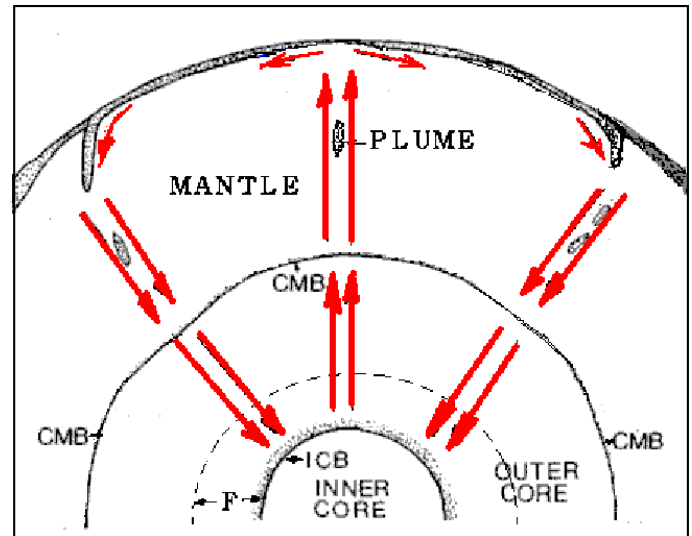


Figure 3. This is a schematic diagram of the great convection cell. A circulation of magma and solid or molten rock migrates up to the crust and down to the F zone of the outer core and causes topography of the core.

According to the description above, the difference in density between the outer core and the inner core must be great. Jeanloz and Ahrens completed shock-wave experiments [Jeanloz & Ahrens, 1980], in which it was found that the density of FeO is 10.14 g/cm³ when reduced to core temperature and 250 GP a pressure and under the same conditions the density of Fe is 12.62 g/cm³ [McQueen *et al.*, 1970]. The difference between both is 2.48 g/cm³, a figure higher than all the previous evaluated values.

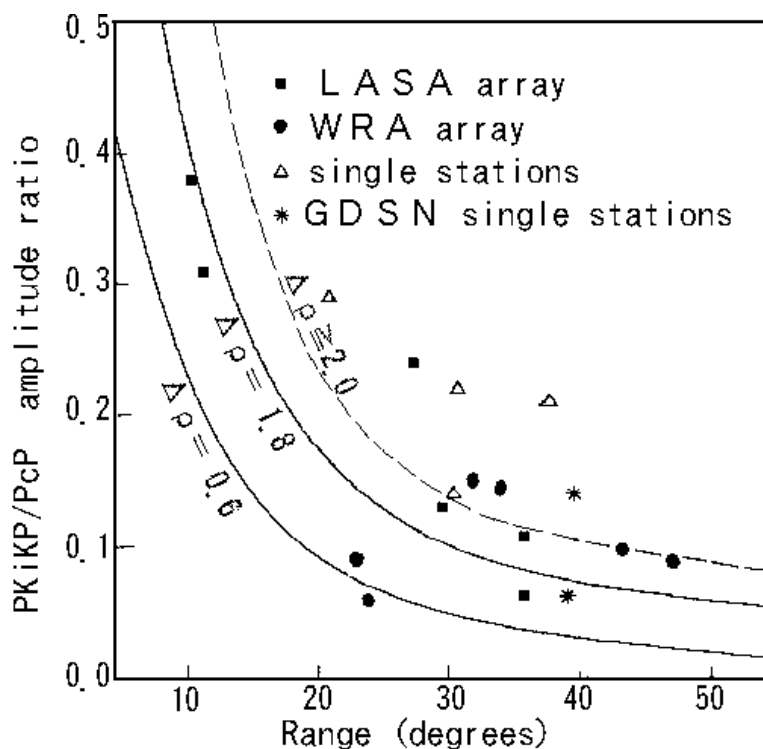


Figure 4. Observed PKiKP/PcP amplitude ratios plotted as a function of range. Solid squares indicate LASA array data [Engdahl *et al.*, 1970, 1974]; open triangles are single-station data [Buchbinder *et al.*, 1973]; solid circles are Warramunga array data [Souriau & Souriau, 1989]; stars are single-station GDSN data [Shearer & Masters, 1990]. The lower curve shows the theoretical amplitude ratio for PREM ($\rho = 0.6$ g/cm³). The middle curve shows the result for a higher density contrast ($\rho = 1.8$ g/cm³). The upper dashed curve shows a more reasonable curve of mean value among all the scattered points for a favorable density contrast ($\rho \geq 2.0$ g/cm³).

Figure 4 plots the PKiKP/PcP observations which contain LASA array data from Engdahl and Flinn [Engdahl *et al.*, 1970; Engdahl *et al.*, 1974], single-station data from Buchbinder [Buchbinder *et al.*, 1973], Warramunga array data from Souriau and Souriau [Souriau & Souriau, 1989], and single-station GDSN data from Shearer and Masters [Shearer & Masters, 1990]. The theoretical amplitude ratio from PREM ($\Delta\rho = 0.6 \text{ g/cm}^3$) is shown, compared with that predicted for a higher ICB density contrast ($\Delta\rho = 1.8 \text{ g/cm}^3$). The data exhibit considerable scatter, but clearly favor models with higher ICB density contrasts than PREM. From Figure 4, one would expect that, on average, the observed PKiKP/PcP amplitude ratios will scatter about the “true” amplitude ratio, so a dashed line ($\Delta\rho \geq 2.0 \text{ g/cm}^3$) is a more reasonable curve of mean value among all the scattered points that indicates a favorable density jump a slightly larger than 2.0 g/cm^3 .

Based on the free oscillation periods, Derr has inferred an earth model DI-11 by least-squares inversion with an average shear velocity of 2.18 km/sec in the innercore and a jump in density of 2 g/cm^3 at its boundary that satisfies the known mass and moment of inertia [Derr, 1969]. We use the density jump of Derr's suggestion 2.0 g/cm^3 at the ICB to research the new earth model in this paper.

IV. The evaluation of the structure of the new earth model

In order to calculate the data of the earth, the density distribution follows the divisions of the PREM divided into 94 levels, including 82 thin shells. The thickness of each shell is not greater than 100 km and so small compared with the earth's radius of 6371 km that the density is regarded as linear variation within it. Then, we use a simplification method to calculate the information of the earth to simplify the calculating work.

The formula for the mass M of a uniform sphere,

$$M = (4/3) \pi \rho R^3 \quad (4)$$

Where R is the radius and ρ is the density.

The mass ΔM of each shell in the earth's interior can be calculated through

$$\Delta M = (4/3) \pi \rho_t R_t^3 - (4/3) \pi \rho_b R_b^3 \quad (5)$$

Where: ρ_t and ρ_b are the densities of the top and the bottom, respectively, in a shell. R_t and R_b are the radii of the top and the bottom in a shell. Because the difference between ρ_t and ρ_b is so small and the density is regarded as linear variation in the shell, the mean value $\bar{\rho}$ of both ρ_t and ρ_b is substituted for ρ_t and ρ_b to simplify the calculation. Then equation (5) becomes.

$$\Delta M = (4/3) \pi \bar{\rho} (R_t^3 - R_b^3) \quad (6)$$

The formula for the moment I of inertia of a uniform sphere,

$$I = (2/5) M R^2 \quad (7)$$

The moment of inertia ΔI of each shell in the earth's interior can be calculated through combining equations (4) and (7),

$$\Delta I = (8/15) \pi \bar{\rho} (R_t^5 - R_b^5) \quad (8)$$

From fluid mechanics, in a region of uniform composition, which is in a state of hydrostatic stress, the gradient of hydrostatic pressure is expressed by

$$dP / dR = -g\rho \quad (9)$$

Where P, R are the pressure and the radius, respectively, at the region; ρ is the density at that depth; g is the acceleration due to gravity at the same depth.

If the effect of the earth's rotation is negligible, the potential theory shows that g is resulted only from the attraction of the mass M within the sphere of radius R through

$$g = GM / R^2 \quad (10)$$

Where: G is the gravitational constant “ $6.6726 \times 10^{-11} \text{ m}^3/\text{kg.s}^2$ ”.

Equation (10) substitutes into equation (9) and we integrate it. To simplify the calculation, we take the mass \bar{m} of a sphere as the mean value of M_t and M_b , which are the masses of the sphere within the top radius R_t and the bottom radius R_b , respectively, of a shell.

$$M_t = (4/3)\pi\bar{\rho}R_t^3 \quad (11)$$

$$M_b = (4/3)\pi\bar{\rho}R_b^3 \quad (12)$$

$$\bar{m} = (M_t + M_b)/2 \quad (13)$$

So, in equations (9) and (10), we take ρ and M as $\bar{\rho}$ and \bar{m} , which are considered the constants in the thin shell and irrelative to the P and R. Then we get

$$\Delta P = (1/R_b - 1/R_t)G\bar{m}\bar{\rho} \quad (14)$$

Where: ΔP is the difference in pressure between the top and the bottom in a layer of the Earth.

Equation (10) cannot be applied to the center of the earth where is a discontinuous point. Combining equations (4), (9) and (10), we integrate and then get

$$\Delta P_c = (2/3)\pi G\bar{\rho}^2 R_c^2 \quad (15)$$

Where: ΔP_c is the difference in pressure between the radius R_c and the center of the earth at the center portion.

The acceleration due to gravity g of each layer can be derived from equation (10). According to the observation data, the moment of inertia about the polar axis of the earth is 0.3309MeRe^2 [Garland, 1979] and about an equatorial axis is 0.3298MeRe^2 . The earth is regarded as a sphere, of which the moment of inertia is determined to be $80286.4 \times 10^{40} \text{ g.cm}^2$ by taking the mean value of both figures, where Me is the earth's mass of $5974.2 \times 10^{24} \text{ g}$ and Re is the equatorial radius of 6378.14 km. To examine the accuracy of applied equations, we apply the density distribution of the PREM to calculate the earth's mass, moment of inertia, pressure and acceleration due to gravity. The calculated values of the earth's data from the density distribution of the Preliminary Reference Earth Mode as compared with the values of the current data and the PREM are listed in Table 1 and Table 2.

Table I. The calculated values of the earth's data from the density distribution of the Preliminary Reference Earth Mode and compared with it.

Level	Radius	Density	Mass within Radius	Moment within Radius	Gravity	Pressure	Pressure Deviation
	R	ρ	M	I	g	P	ΔP
No	km	g/cm^3	10^{24} g	10^{40} g.cm ²	10^3 cm/s ²	Kbar	10^{-3}
94	6371.0	1.02000	5973.289	80205.664	981.959	0.000	0.000
93	6368.0	1.02000	5971.729	80163.472	982.628	0.301	5.211
92	6368.0	2.60000	5971.729	80163.472	982.628	0.301	8.053
91	6356.0	2.60000	5955.860	79735.267	983.721	3.368	1.215
90	6356.0	2.90000	5955.860	79735.267	983.721	3.368	0.568
89	6346.6	2.90000	5942.042	79363.655	984.348	6.051	1.744
88	6346.6	3.38076	5942.042	79363.655	984.348	6.051	1.247
87	6331.0	3.37906	5915.418	78650.501	984.772	11.242	0.255
86	6311.0	3.37688	5881.498	77746.958	985.341	17.897	0.328
85	6291.0	3.37471	5847.813	76855.371	985.937	24.552	0.510
84	6291.0	3.37471	5847.813	76855.371	985.937	24.552	0.225
83	6256.0	3.37091	5789.430	75323.498	987.046	36.197	0.387
82	6221.0	3.36710	5731.761	73827.216	988.241	47.843	0.395
81	6186.0	3.36330	5674.801	72365.862	989.523	59.490	0.410
80	6151.0	3.35950	5618.547	70938.843	990.895	71.140	0.453
79	6151.0	3.43578	5618.547	70938.843	990.895	71.140	0.354
78	6106.0	3.46264	5545.290	69104.504	992.443	86.533	0.413
77	6061.0	3.48951	5472.542	67309.578	994.021	102.070	0.417
76	6016.0	3.51639	5400.312	65553.702	995.631	117.752	0.421
75	5971.0	3.54325	5328.609	63836.530	997.275	133.580	0.447
74	5971.0	3.72378	5328.609	63836.530	997.275	133.580	0.394
73	5921.0	3.78678	5245.188	61870.242	998.311	152.315	0.422
72	5871.0	3.84980	5161.788	59937.364	999.243	171.384	0.426
71	5821.0	3.91282	5078.443	58038.407	1000.070	190.784	0.427
70	5771.0	3.97584	4995.188	56173.776	1000.794	210.515	0.430
69	5771.0	3.97584	4995.188	56173.776	1000.794	210.515	0.425
68	5736.0	3.98399	4937.243	54894.999	1001.293	224.460	0.427
67	5701.0	3.99214	4879.884	53644.500	1001.849	238.440	0.445
66	5701.0	4.38071	4879.884	53644.500	1001.849	238.440	0.412
65	5650.0	4.41241	4789.122	51695.390	1001.046	260.896	0.434
64	5600.0	4.44316	4701.095	49838.510	1000.272	283.051	0.437
63	5600.0	4.44317	4701.095	49838.510	1000.272	283.051	0.434
62	5500.0	4.50372	4527.934	46282.178	998.780	327.772	0.454
61	5400.0	4.56307	4358.719	42930.977	997.393	373.027	0.470
60	5300.0	4.62129	4193.543	39778.675	996.149	418.809	0.485
59	5200.0	4.67844	4032.484	36818.780	995.087	465.113	0.497
58	5100.0	4.73460	3875.615	34044.639	994.249	511.936	0.509
57	5000.0	4.78983	3722.994	31449.399	993.682	559.281	0.518
56	4900.0	4.84422	3574.669	29026.105	993.433	607.151	0.528
55	4800.0	4.89783	3430.681	26767.722	993.557	655.55Q	0.537
54	4700.0	4.95073	3291.058	24667.171	994.111	704.504	0.547
53	4600.0	5.00299	3155.823	22717.392	995.158	754.016	0.555
52	4500.0	5.05469	3024.990	20911.315	996.768	804.113	0.564
51	4400.0	5.10590	2898.564	19241.931	999.016	854.820	0.572
50	4300.0	5.15669	2776.543	17702.299	1001.988	906.171	0.579
49	4200.0	5.20713	2658.919	16285.574	1005.777	958.203	0.587
48	4100.0	5.25729	2545.676	14985.041	1010.487	1010.963	0.594
47	4000.0	5.30724	2436.792	13794.099	1016.234	1064.504	0.602
46	3900.0	5.35706	2332.241	12706.303	1023.150	1118.888	0.609

45	3800.0	5.40681	2231.989	11715.364	1031.383	1174.188	0.616
44	3700.0	5.45657	2135.997	10815.178	1041.100	1230.486	0.624
43	3630.0	5.49145	2071.317	10235.887	1048.886	1270.533	0.624
42	3630.0	5.49145	2071,317	10235.887	1048.886	1270.533	0.623
41	3600,0	5.50642	2044.225	9999.856	1052.492	1287.866	0.621
40	3500.0	5.55641	1956.620	9263.582	1065.775	1346.464	0.628
39	3480.0	5.56645	1939.595	9125.339	1068.680	1358.335	0.609
38	3480.0	9.90349	1939.595	9125.339	1068.680	1358.335	0.608
37	3400.0	10.02940	1821.025	8189.719	1051.122	1442.882	0.652
36	3300.0	10.18134	1678.502	7123.015	1028.464	1548.038	0.682
35	3200.0	10.32726	1542.384	6164.138	1005.050	1652.385	0.712
34	3100.0	10.46727	1412.729	5306.115	980.913	1755.720	0.742
33	3000.0	10.60152	1289.573	4541.998	956.089	1857.844	0.773
32	2900,0	10.73012	1172.922	3864.903	930.611	1958.564	0.804
31	2800.0	10.85321	1062.760	3268.068	904.512	2057.694	0.835
30	2700.0	10.97091	959.048	2744.899	877.825	2155.056	0.867
29	2600.0	11.08335	861.725	2288.994	850.584	2250.478	0.901
28	2500.0	11,19067	770.709	1894.191	822.821	2343.794	0.936
27	2400.0	11.29298	685.901	1554.580	794.573	2434.847	0.971
26	2300.0	11.39042	607.181	1264.538	765.875	2523.487	1.010
25	2200.0	11,48311	534.411	1018.739	736.758	2609.572	1.049
24	2100.0	11.57119	467.440	812.171	707.265	2692.969	1.091
23	2000.0	11.65478	406.100	640.145	677.436	2773.552	1.135
22	1900.0	11.73401	350.208	498.303	647.312	2851.205	1.182
21	1800.0	11.80900	299.568	382.619	616.944	2925.821	1.232
20	1700.0	11.87990	253.973	289.403	586.388	2997.305	1.285
19	1600.0	11.94682	213.202	215.291	555.708	3065.572	1.343
18	1500.0	12.00989	177.026	151.249	524.988	3130.550	1.405
17	1400.0	12.06924	145.204	112.556	494.331	3192.185	1.472
16	1300.0	12,12500	117.486	78.802	463.868	3250.438	1.545
15	1221.5	12,16634	98.436	58.583	440.212	3293.691	1.578
14	1221.5	12.16360	98.436	58.583	440.212	3293.691	1.571
13	1200.0	12.77493	93.378	53.640	432.690	3305.677	1.575
12	1100.0	12.82501	72.093	34.814	397.560	3359,210	1.674
11	1000.0	12.87073	54.279	21.671	362.182	3408.454	1.784
10	900.0	12.91211	39.646	12.826	326.595	3453.339	1.908
9	800.0	12.94912	27.892	7.132	290.800	3493.806	2,048
8	700.0	12.98178	18.714	3.665	254.839	3529.806	2.210
7	600.0	13.01009	11.800	1.698	218.713	3561.307	2.399
6	500.0	13.03404	6.836	0.684	182.456	3588.295	2.627
5	400.0	13.05364	3.503	0.224	146.088	3610.792	2,910
4	300.0	13.06888	1.479	0.054	109.653	3628.883	3.282
3	200.0	13.07977	0,438	0.007	73.065	3642.820	3.820
2	100.0	13.08630	0.055	0.001	36,699	3653.579	4,799
1	0.0	13.08848	0.000	0.000	0.000	3655.973	4.796

Table 2. The calculated values from the density distribution of the PREM are compared with the current data and the PREM.

Data of the Earth	Mass	Moment of inertia	Pressure at CMB	Pressure At Earth center	Gravity at CMB	Gravity at Earth surface
Unit	10^{24} g	10^{40} g.cm ²	K bar	K bar	cm/sec ²	cm/sec ²
PREM & Current	5974.200	80286.400	1357.509	3638.524	1068.230	981.560
Calculated values	5973.289	80205.664	1358.335	3655.973	1068.680	981.959
Difference %	-0.0152	-0.1006	+0.0608	+0.4796	+0.0421	+0.0406

The calculated earth's mass, as indicated in Table 1, is 5973.289×10^{24} g, which is 0.0152 % less than the current value of 5974.2×10^{24} g. The calculated moment of inertia is 80205.664×10^{40} g.cm², which is 0.1006 % less than the average observation value of 80286.4×10^{40} g.cm². The deviations of interior gravity are about 0.042 %, with the middle portion exception. The interior pressure is 1358.335 kbar at the CMB, which is 0.0608 % higher than the PREM value of 1357.509 kbar. These comparisons indicate that the calculated data are close to the current values. It proves that the simplification method is acceptable and useful. However, the pressure of 3655.973 kbar is higher than the PREM value of 3638.524 kbar by 0.4796 % at the earth's center about 8 times of the deviation at the CMB. We compare all the calculated pressures of the simplification method with the pressures of the PREM. The deviation E of the calculated pressure from the pressure P of the PREM is shown in Figure 5.

From the crust to the CMB, the deviations are drawn as a straight line E which indicates the calculated pressures of the simplification method have a system error in view of the error theory compared with those of the PREM. But from the CMB to the earth's center, the deviations of the calculated pressure from those of the PREM sharply increase above the system deviation — the dashed line. This indicates that there is considerable discrepancy between the two methods only within the core related to the pressure. We could confirm that the structure of the core in the PREM, which affects its pressure, is something incorrect.

To investigate the structure of the earth — particularly the core, the density distribution of the PREM is adapted from the crust to the CMB. As described

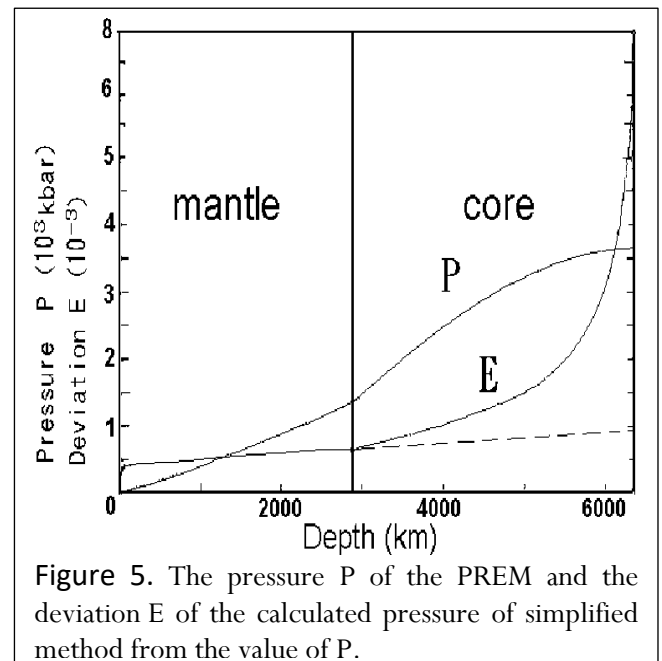


Figure 5. The pressure P of the PREM and the deviation E of the calculated pressure of simplified method from the value of P .

above, the components of the outer core are like those in the lower mantle, and the density distributions between both are continuous at the CMB. Then from the CMB to the ICB, four differently plotted density curves are set to match the known conditions. Due to a small jump of P-wave velocity at the boundary of F transition zone in the outer core, the slope of density curve is as steep as the PREM. There is a discontinuity at the ICB,

so that a density jumps of 2.0 g/cm^3 is used there. In the inner core, the same slope of density curve of the PREM is used in this portion. The four density curves of the assumed earth model compared with the PREM are shown in Figure 6.

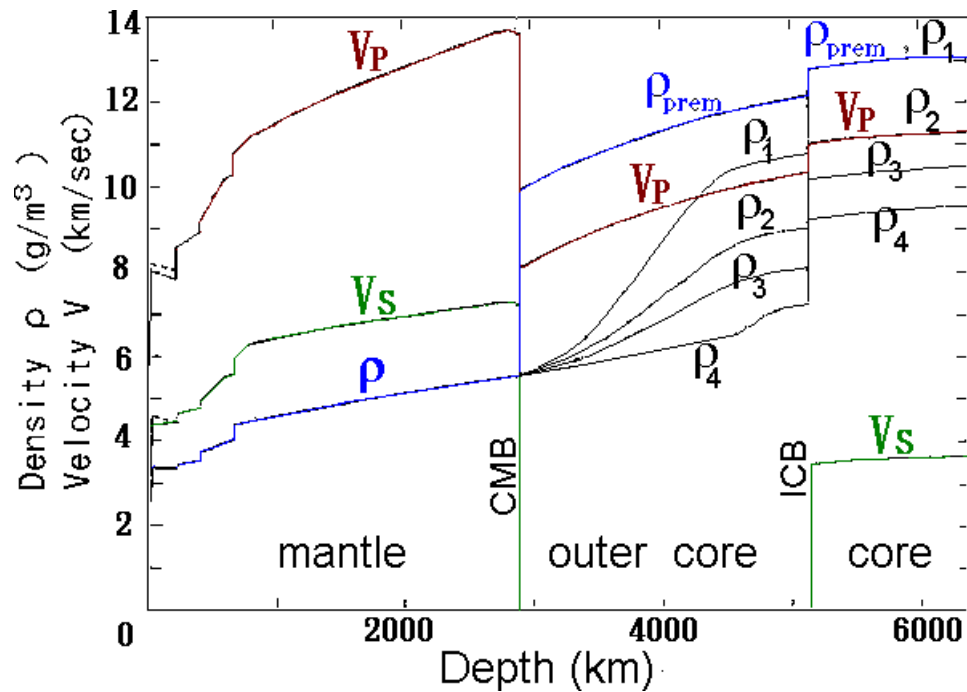


Figure 6. The density ρ of the new Earth models 1, 2, 3 and 4 compared with the PREM.

From equations (6) and (8), the mass and the moment of inertia of the four new earth models can be determined. These are compared with the observed values of the earth's mass $5974.2 \times 10^{24} \text{ g}$ and moment of inertia $80286.4 \times 10^{40} \text{ g.cm}^2$, and then the differences will be found to be large as Table 3 is shown. The differences are the insufficiencies of the mass and the moment of inertia of the four new earth models.

The insufficiencies of the mass and the moment of inertia can only be obtained by comparing the observation data of the earth but cannot be detected directly. The insufficiency of mass, called the missing mass, belongs to dark matter in astrophysics. The missing mass and moment of inertia of the earth, relative to the gravity, cannot be answered clearly through the ordinary earth sciences. So, a new study of the earth is being attempted by utilizing the contemporary physics

Table 3. The insufficiencies of the mass and the moment of inertia in the four new earth models are showed.

Earth model	Unit	Observed value	New model 1	Newmod. 2	New mod. 3	New mod. 4
Mass	10^{24} g	5974.200	5409.024	5268.126	5204.761	5121.820
Insufficiency	10^{24} g	-	565.176	706.074	769.439	852.380
Moment of inertia	10^{40} g.cm^2	80286.400	77007.472	76571.028	76378.768	76126.841
Insufficiency	10^{40} g.cm^2	-	3278.928	3715.372	3907.632	4159.559

There are two types of dark matter: hot dark matter (HDM) and cold dark matter (CDM). Hot dark matter exists as such in a kind of photon or neutrino which has zero mass and moves at or approaching the speed of light. Cold dark matter exists at a lower energy and particle type. Due to the gravity of the particles, CDM moves at a low speed and collects like normal matter. According to the observation data of background radiation in the universe, some physicists have recently proposed that cold dark matter explains the cosmic structure. Blumenthal argued that the CDM model for the formation and distribution of galaxies in the universe is successful and the expansion of the universe is dominated by the CDM [Blumenthal *et al.*, 1984]. After reporting the South Pole experiment, Lubin showed that according to a recent anisotropy experiment in which a Bayesian analysis was used to constrain the amplitude of the perturbation spectrum, they showed that adiabatic HDM models were convincingly ruled out and CDM models had anisotropies near their derived limits [Lubin *et al.*, 1991]. Based on the result of their experiment, they announced the South Pole experiment was particularly well suited to the CDM-type model, among others.

We proceed with the assumption that the missing mass and moment of inertia of the earth are those of dark matter which may constitute a normal planet of the CDM. To find some solution in this article, dark matter is compared to Mars. The average radius of Mars is 3397 km, and the mass is 642.40×10^{24} g. Its mass approaches the insufficient mass of the new earth model (2) in the Table 3. So, dark matter is considered as a planet, called a dark planet, of which the form is like Mars and its characteristics are based on the inner planets of the solar system. The data of the dark planet can be calculated as follows.

A dark planet is considered as a sphere, whose radius and density can be calculated through the insufficiency of the mass and the moment of inertia of the earth. The moment of inertia of a sphere can be derived through

$$I = CMR^2 \quad (16)$$

Where C is the coefficient of the moment of inertia, which is 0.4 in a uniform sphere as equation (4) showed. From experience, the four dark planets are each individually given the trial values of C such as $0.33 \sim 0.4$ to determine the approximate radii of the dark planets through equation (16). To consider the density of rock on the surface of the earth and the moon, we assume that the surface density of the dark planet is 2.70 g/cm^3 . Under the condition that the density of a layer is proportional to its depth, we select a trial value of density at the center of dark planet and apply equations (6) and (8) to calculate the mass and the moment of inertia of each shell and the total mass and moment of inertia. Because the radius and the center density of the dark planet are the hypothetical values, but the total mass and moment of inertia are necessary to correspond to the insufficiency of the earth's mass and moment of inertia; therefore, it is necessary to use a trial-and-error approach to determine the proper radius and center density. Then, we calculate the average density of the dark planet through equation (4).

To search for the location of the dark planet in the universe, we apply the most advanced physical theory — “Superstring theory”, to solve the problem. Superstring theory attempts a broader exploration than Einstein's Relativity theory. This theory is deduced from the characteristics of String theory and Supersymmetry and the most promising hope for truly unifying the scale of the microcosm and the macrocosm, which completes the descriptions of both in quantum field theory and General Relativity. Crudely speaking, it can unify the four

basic interacting forces of nature and various elementary particles of the universe. This theory, a candidate for “theory of everything”, is based on the universe constitution of nine-dimensional space and one-dimensional time and has Supersymmetry of $E_8 \times E_8$. However, Superstring theory, called ten-dimensional theory, is now not established as well as Relativity theory. The problem rests with the former's failure, as far as working out a theoretically solid basic geometry is overly concerned. Because there is not the exact boundary condition to fit the real universe, though many mathematicians and physicists have attempted to break the constitution of ten-dimensional space-time model down to a four-dimensional one as our known world, no proposed method meets perfection.

At Harvard University (Oct. 29, 1987), the renowned cosmologist — Professor A. Linde, lectured that since the universe was produced from the “Big Bang”, ten-dimensional space-time of the universe is unnecessarily compactified (broken down) into a four-dimensional space-time, and other number of dimensional space-time may exist. Supersymmetry is one of the most elegant of all symmetries, although there is no empirical data to support the notion of highly desirable theoretical mechanisms that hold tremendous promise. But Hall reported that the physicists of CERN announced the first experimental evidence for Supersymmetry [Hall, 1991]. According to Supersymmetry, every dimension of nine-dimensional space must have the property of global symmetry with equivalent mathematical weight, so every dimension is all symmetric. The universe need not be compactified into the local symmetry when its vacuum high-energy phase transits into a low-energy one.

Without breaking the nine-dimensional space of the universe down, the ten-dimensional space-time is considered to universally exist. Time cannot be divided into some distinct parts, so one-dimensional time is taken as a common standard in order of event in the universe. According to the “anthropic principle”, three-dimensional space and one-dimensional time are taken as one cosmos as our living world; therefore, the nine-dimensional space can be divided into three portions, and each portion has a common standard time, which are considered as there are three cosmoses in the universe. In other word, the framework of the universe, containing nine-dimensional space and one-dimensional time, will be established as a three-cosmic structure. The dark planet can be situated in a cosmos other than our own. The structure of the three-cosmic universe cannot be observed directly but can be recognized from the “missing neutrinos of the sun”.

According to Superstring theory, the $E_8 \times E_8$ supersymmetric structure has characteristics in which each E_8 represents a single symmetrical group. One E_8 describes a world of general matter and the other E_8 describes a world of shadow matter. There are no basic interactive forces between any two different cosmoses except for gravity. Therefore, among the three cosmoses, only the force of gravity can affect the entire universe. In other words, the theoretic graviton in the field of gravity can penetrate all three cosmoses; however, photon cannot penetrate through other cosmoses. The graviton has been observed by the researchers in a global network, but they have not caught yet. The graviton has the physical characteristics: rest mass = 0, charge = 0, spin = 2 and the speed of light. The lepton — neutrino, which has been captured, has the physical characteristics: rest mass = 0, charge = 0, spin = 1/2 and the speed of light. The neutrino and the graviton carry a very small amount of energy. The neutrino is fermions, and the lepton is boson. Supersymmetry is one of the most elegant of all symmetries, which unites bosons and fermions into a single multiplet and describes both

are the same kind of particle. So, the physical characteristics of neutrino and the graviton are like each other. Less than 2 % of the sun's energy is emitted in the form of neutrinos. Only about one-third the amount of the neutrinos can be caught on the earth as the astrophysical theory predicts, and about two-thirds of it disappears. This solar- neutrino problem has been a big mystery in Astro-particle physics for the past three decades. Since the graviton can penetrate all the three cosmoses as the physical theory describes, if we compare the neutrino to the graviton, the neutrinos of the sun should uniformly emit into all the three cosmoses. They reach the cosmos of our world only one-third of their original amount and the other two-thirds of it should emit into the other two cosmoses. Therefore, not only the problem of the solar-neutrino problem could be solved, but also the three cosmoses of the universe structure will be proved indirectly.

According to the three-cosmic structure of the ten-dimensional space-time universe model, all the normal matter of CDM should exist in the three cosmoses. So, the South Pole experiment which predicted the CDM model of the cosmic-structure also supports the three-cosmic structure.

Superstring theory argues that there are no interacting forces, including the electromagnetic force, between any two cosmoses except gravity, so the dark planet which is found through the gravity force should be in another invisible cosmos. The earth orbits around the sun and the orbit may be affected by the gravity of the dark planet, but no abnormal effect has been observed. Therefore, we assume that the gravitycenters of the earth and the dark planet coincide with each other at one point but in different cosmos. Based on the effect in which the same side of the moon always facesthe earth while revolving around the earth, we infer that the dark planet and the earth should rotate synchronously. It is hard to examine the existence of dark planet directly, however, it can be observed from “Chandler wobbles.”

Referring to the orientation of the rotation axis of the earth in space in addition to both precession and nutation, there is a wobble on the instantaneous axis of rotation of the earth itself. The wobble alters the position of a point on the earth relative to the pole of rotation. Chandler pointed out that there are two distinct kinds of the wobble periods. One is a period of 12 months, and the other is a period of 14 months [Chandler, 1891]. The former, called annual wobble, is obviously affected by the seasonal climate. The latter, called Chandler wobble, has not been solved for a hundred years. We have postulated that both the earth and the dark planet spin synchronously around the same gravity center, but the rotation axes of both are impossible coinciding with each other. In other words, an angle between the two rotation axes produces the Chandler wobble as the precession and nutation because of the sun and the moon on non-parallel axes. Therefore, the problem of Chandler wobble should be solved and indirectly confirms the existence of dark planet inside the earth.

Assuming that the gravity centers of the earth planet and the dark planet coincideat a single point, and both rotate synchronously, the global mass and moment of inertiais be obtained from the sum of them. Based on mechanics, the gravity at each shell inside the earth is affected by the mass of the earth and the dark planet within its radius. From equation (10), the pressure difference $\Delta P'$ between the top and the bottom of a shell within the earth is calculated through

$$\Delta P' = (1/R_b - 1/R_t)G \bar{M}' \bar{\rho} \quad (17)$$

Where \bar{M}' is the mean value of the total mass of the earth, and the dark planet is within the radius R_t

and R_b . $\bar{\rho}$ is the mean density in this layer of the earth.

Equation (17) cannot be applied to the earth's center, because there is a discontinuous point. From equation (4), the average density $\bar{\rho}'$ of the middle portion of the earth combined with the dark planet within its radius R_c can be calculated through

$$\bar{\rho}' = (M_c + M_d) / [(4/3) \pi R_c^3] \quad (18)$$

Where: M_c and M_d are the masses of middle portion in the earth and in the dark planet, respectively.

From equations (18), (9) and (10), the differences of pressure between the top and the center of the middle portion in the earth can be obtained through

$$\Delta P'_c = (2/3) \pi G \bar{\rho} \bar{\rho}' R_c^2 \quad (19)$$

To calculate the pressure of the earth, we use the density of the earth only, in other words, the weight per unit volume at each depth within the earth; for example, we use $\bar{\rho}$ in equations (17) and (19). But to calculate the gravity force, we must use the masses of both the earth and the dark planet; for example, we use \bar{M}' in equation (17) and $\bar{\rho}'$ in equation (19). The pressure in each layer can be obtained by adding the pressure differences of each layer from the surface layer to this layer. The pressure of the earth's center is the sum of all the pressure differences of every layer of the earth.

Based on the characteristics of the inner planets of the solar system, besides Mercury, the bigger the radius of a planet is, the higher the average density. So, the radius and the average density of a suitable dark planet must be compatible with the characteristics of inner planet in solar system. After calculation, the data of the four new earth models and each dark planet are compared with the data of the current earth and the PREM listed in the Table 4. We find a more suitable dark planet belonging to the new earth model (4), whose radius and average density both are bigger than those of Mars. In this model the slope of density curve from a depth of 400 km of the upper mantle through zones C, D and E to the upper boundary of F zone is nearly a straight line, which means the density increase in proportion to its depth in accord with general physical phenomenon. So, the new earth model (4) is acceptable as the proper “new earth model”.

Table 4. The calculated data of the four new earth models compared with the data of the current earth and the PREM.

Kind of Earth's model	The earth planet							The dark planet					Suitability
	Radius	Ave. density	Mass of Earth	Moment of inertia	Center density	Center pressure	Moment of inertia	Radius	Ave. density	Mass	Moment of inertia	Moment of inertia	
	km	g/cm ³	10 ²⁴ g	10 ⁴⁰ g.cm	g/cm ³	kbar	C	km	g/cm ³	10 ²⁴ g	10 ⁴⁰ g.cm	C	
PREM	6371	5.5150	5974.200	80286.400	13.08848	3638.524	0.3309						
Model 1	6371	4.9935	5409.024	77007.472	13.08848	3283.754	0.3508	3808.414	2.4427	565.176	3278.928	0.4000	no
Model 2	6371	4.8635	5268.126	76571.028	11.29785	3039.584	0.3581	3732.304	3.2421	706.074	3715.372	0.3777	no
model 3	6371	4.8050	5204.761	76378.768	10.46002	2934.587	0.3615	3717.755	3.5747	769.439	3907.632	0.3674	no
model 4	6371	4.7284	5121.820	76126.841	9.49821	2805.297	0.3662	3700.375	4.0161	852.380	4159.559	0.3564	good

The precise data of the earth and the dark planet are calculated from the density distribution of the new earth model and listed in Tables 5, 6 and 7. The pressure P and the acceleration due to gravity g of the new earth model compared with the PREM are shown in Figure 7. We can find the pressure curve of the

new earth model is smoother than that of the PREM below the CMB. In the gravity curve of the new earth model, there are two deflection points in the curve which the one is at 2670.625 km in depth at the radius of the dark planet, and the other is at the ICB.

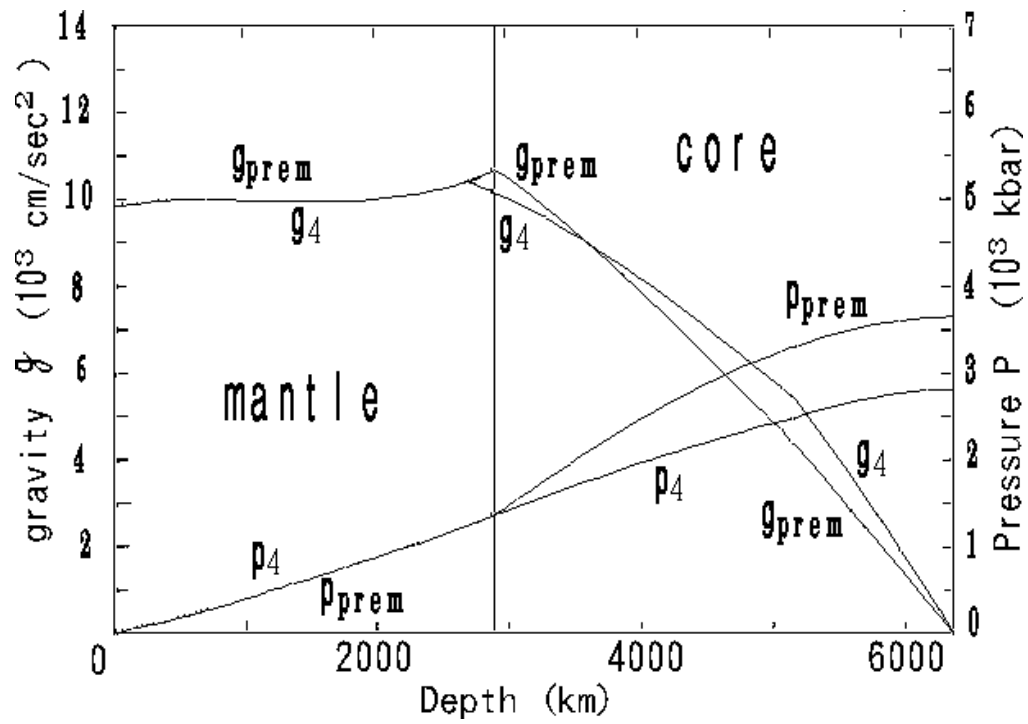


Figure 7. The gravity g and the pressure P of the new earth model and the PREM.

Table 5. The data of the earth planet of the new earth model are showed.

Le- vel	Radius	Density	Mass of shell	Moment of Inertia	Le- vel	Radius	Density	Mass of shell	Moment of Inertia
No.	km	g/cm ³	10 ²⁴ g	10 ⁴⁰ g.cm ²	No.	km	g/cm ³	10 ²⁴ g	10 ⁴⁰ g.cm ²
94	6371.0	1.02000			47	4000.0	5.30724	108.883	1190.942
93	6368.0	1.02000	1.560	42.192	46	3900.0	5.35706	104.551	1087.797
92	6368.0	2.60000	0.000	0.000	45	3800.0	5.40681	100.252	990.939
91	6356.0	2.60000	15.869	428.205	44	3700.0	5.45657	95.991	900.186
90	6356.0	2.90000	0.000	0.000	43	3630.0	5.49145	64.681	579.291
89	6346.6	2.90000	13.818	371.612	42	3630.0	5.49145	0.000	0.000
88	6346.6	3.38076	0.000	0.000	41	3600.0	5.50642	27.091	236.031
87	6331.0	3.37906	26.623	713.154	40	3500.0	5.55641	87.605	736.274
86	6311.0	3.37688	33.921	903.543	39	3480.0	6.56645	17.025	138.243
85	6291.0	3.37471	33.885	891.587	38	3400.0	5.60987	66.482	524.600
84	6291.0	3.37471	0.000	0.000	37	3300.0	5.66415	79.503	595.032
83	6256.0	3.37091	58.383	1531.873	36	3200.0	5.71843	75.548	532.191
82	6221.0	3.36710	57.669	1496.283	35	3100.0	5.77270	71.647	474.147
81	6186.0	3.36330	56.960	1461.353	34	3000.0	5.82698	67.805	420.694
80	6151.0	3.35950	56.254	1427.019	33	2900.0	5.88126	64.026	371.635
79	6151.0	3.43578	0.000	0.000	32	2800.0	5.93553	60.313	326.765
78	6106.0	3.46264	73.258	1834.339	31	2700.0	5.98981	56.671	285.875
77	6061.0	3.48951	72.748	1794.926	30	2600.0	6.04409	53.104	248.764
76	6016.0	3.51639	72.230	1755.876	29	2500.0	6.09837	49.616	215.223
75	5971.0	3.54325	71.702	1717.172	28	2400.0	6.15264	46.211	185.049
74	5971.0	3.72378	0.000	0.000	27	2300.0	6.20692	42.893	158.036
73	5921.0	3.78678	83.421	1966.289	26	2200.0	6.26120	39.666	133.982
72	5871.0	3.84980	83.400	1932.878	25	2100.0	6.31547	36.534	112.688
71	5821.0	3.91282	83.344	1898.957	24	2000.0	6.36975	33.502	93.955
70	5771.0	3.97584	83.256	1864.631	23	1900.0	6.42403	30.573	77.588
69	5771.0	3.97584	0.000	0.000	22	1800.0	6.47831	27.752	63.398
68	5736.0	3.98399	57.945	1278.777	21	1787.5	6.48509	3.276	7.027
67	5701.0	3.99214	57.359	1250.499	20	1700.0	6.52703	21.757	44.150
66	5701.0	4.38071	0.000	0.000	19	1600.0	6.88649	22.952	41.722
65	5650.0	4.41241	90.762	1949.III	18	1500.0	7.03784	21.027	33.736
64	5600.0	4.44316	88.027	1856.879	17	1400.0	7.09459	18.677	26.231
63	5600.0	4.44317	0.000	0.000	16	1300.0	7.15135	16.321	19.875
62	5500.0	4.50372	173.161	3556.332	15	1221.5	7.17442	11.235	11.924
61	5400.0	4.56307	169.215	3351.201	14	1221.5	9.17442	0.000	0.000
60	5300.0	4.62129	165.176	3152.302	13	1200.0	9.18575	3.636	3.554
59	5200.0	4.67844	161.058	2959.895	12	1100.0	9.23583	15.317	13.547
58	5100.0	4.73460	156.869	2774.141	11	1000.0	9.28155	12.837	9.471
57	5000.0	4.78983	152.621	2595.240	10	900.0	9.32293	10.560	6.383
56	4900.0	4.84422	148.325	2423.294	9	800.0	9.35994	8.491	4.113
55	4800.0	4.89783	143.989	2258.383	8	700.0	9.39260	6.638	2.507
54	4700.0	4.95073	139.623	2100.552	7	600.0	9.42091	5.004	1.423
53	4600.0	5.00259	135.234	1949.779	6	500.0	9.44486	3.596	0.735
52	4500.0	5.05469	130.833	1806.076	5	400.0	9.46446	2.416	0.333
51	4400.0	5.10590	126.426	1669.385	4	300.0	9.47970	1.468	0.124
50	4300.0	5.15669	122.021	1539.631	3	200.0	9.49059	0.755	0.034
49	4200.0	5.20713	117.625	1416.725	2	100.0	9.49712	0.278	0.005
48	4100.0	5.25729	113.243	1300.533	1	0.0	9.49821	0.040	0.000
Total								5,121.820	76,126.841
Insufficiency								852.380	4,159.559

Table 6. The data of the dark planet of the new earth model are showed.

Le- -vel	Radius	Density	Mass of shell	Moment of Inertia	Le- -vel	Radius	Density	Mass of shell	Moment of Inertia
No.	km	g/cm ³	10 ²⁴ g	10 ⁴⁰ g.cm ²	No.	km	g/cm ³	10 ²⁴ g	10 ⁴⁰ g.cm ²
45	3700.375	2.70000							
44	3700	2.70053	0.174	1.590	22	1800	5.40184	22.932	52.388
43	3030	2.80006	32.497	291.052	21	1787.5	5.41961	2.7351	5.860
42	3030	2.80006	0.000	0.000	20	1700	6.64401	8.3321	37.199
41	3600	2.84271	13.900	121.102	19	1600	6.68619	9.2161	34.931
40	3500	2.98488	46.148	387.849	18	1500	6.82836	7.3881	27.897
39	3480	3.01332	9.181	74.550	17	1400	6.97063	6.6931	21.899
38	3400	3.12706	36.526	288.220	16	1300	6.11271	3.843	16.858
37	3300	3.26923	45.106	337.590	15	1221.5	6.22431	9.675	10.269
36	3200	3.41140	44.340	312.352	14	1221.5	6.22431	0.000	0.000
35	3100	3.55358	43.427	287.389	13	1200	6.25488	2.471	2.415
34	3000	3.69575	42.376	262.917	12	1100	6.39706	10.520	9.304
33	2900	3.83792	41.198	239.129	11	1000	6.53923	8.968	6.616
32	2800	3.98010	39.904	216.189	10	900	6.68140	7.604	4.536
31	2700	4.12227	38.504	194.231	09	800	6.82358	6.138	2.973
30	2600	4.26445	37.010	173.370	08	700	6.96676	4.881	1.844
29	2500	4.40662	35.431	153.693	07	600	7.10793	3.743	1.005
28	2400	4.54879	33.780	135.269	06	500	7.26010	2.736	0.559
27	2300	4.69097	32.066	118.145	05	400	7.39227	1.871	0.258
26	2200	4.83314	30.300	102.346	04	300	7.63445	1.167	0.098
25	2100	4.97532	28.493	87.885	03	200	7.67662	0.605	0.027
24	2000	5.11749	26.655	74.754	02	100	7.81880	0.227	0.004
23	1900	5.25966	24.798	62.933	01	0	7.96097	0.033	0.000
Total								852.380	4,159.559

Table 7. The global data of the new earth model are showed.

Le- vel	Radius	Density	Mass of shell	Mass Within Radius	Moment of Inertia	Moment within Radius	Pressure	Gravity
No.	km	g/cm ³	10 ²⁴ g	10 ²⁴ g	10 ⁴⁰ g.cm ²	10 ⁴⁰ g.cm ²	k bar	cm/s ²
94	6371.0	1.02000		5974.200		80286.400	0.000	982.108
93	6368.0	1.02000	1.560	5972.640	42.192	80244.208	0.301	982.778
92	6368.0	2.60000	0.000	5972.640	0.000	80244.208	0.301	982.778
91	6356.0	2.60000	15.869	5956.771	428.205	79816.003	3.369	983.871
90	6356.0	2.90000	0.000	5956.771	0.000	79816.003	3.369	983.871
89	6346.6	2.90000	13.818	5942.953	371.612	79444.391	6.051	984.499
88	6346.6	3.38076	0.000	5942.953	0.000	79444.391	6.051	984.499
87	6331.0	3.37906	26.623	5916.330	713.154	78731.237	11.244	984.924
86	6311.0	3.37688	33.921	5882.409	903.543	77827.694	17.900	985.494
85	6291.0	3.37471	33.685	5848.724	891.587	76936.107	24.555	986.091
84	6291.0	3.37471	0.000	5848.724	0.000	76936.107	24.555	986.091
83	6256.0	3.37091	58.383	5790.341	1531.873	75404.234	36.203	987.201
82	6221.0	3.36710	57.669	5732.672	1496.283	73907.952	47.850	988.398
81	6186.0	3.36330	56.960	5675.712	1461.353	72446.598	59.500	989.682
80	6151.0	3.35950	56.254	5619.458	1427.019	71019.579	71.151	991.056
79	6151.0	3.43578	0.000	5619.458	0.000	71019.579	71.151	991.056
78	6106.0	3.46264	73.258	5546.201	1834.339	69185.240	86.546	992.606
77	6061.0	3.48951	72.748	5473.453	1794.926	67390.314	102.086	994.187
76	6016.0	3.51639	72.230	5401.223	1755.876	65634.438	117.771	995.799
75	5971.0	3.54325	71.702	5329.521	1717.172	63917.266	133.601	997.445
74	5971.0	3.72378	0.000	5329.521	0.000	63917.266	133.601	997.445
73	5921.0	3.78678	83.421	5246.099	1966.289	61950.978	152.340	998.485
72	5871.0	3.84980	83.400	5162.699	1932.878	60018.100	171.412	999.419
71	5821.0	3.91282	83.344	5079.354	1898.957	58119.143	190.816	1000.250
70	6771.0	3.97584	83.256	4996.099	1864.631	56254.512	210.551	1000.977
69	5771.0	3.97584	0.000	4996.099	0.000	56254.512	210.551	1000.977
68	5736.0	3.98399	57.945	4938.154	1278.777	54975.735	224.498	1001.478
67	5701.0	3.99214	57.359	4880.795	1250.499	53725.236	238.480	1002.036
66	5701.0	4.38071	0.000	4880.795	0.000	53725.236	238.480	1002.036
65	5650.0	4.41241	90.762	4790.033	1949.111	51776.126	260.941	1001.237
64	5600.0	4.44316	88.027	4702.006	1856.879	49919.246	283.099	1000.466
63	5600.0	4.44317	0.000	4702.006	0.000	49919.246	283.099	1000.466
62	5500.0	4.50372	173.161	4528.845	3556.332	46362.914	327.829	998.981
61	5400.0	4.56307	169.215	4359.630	3351.201	43011.713	373.094	997.602
60	5300.0	4.62129	165.176	4194.454	3152.302	39859.411	418.886	996.366
59	5200.0	4.67844	161.058	4033.396	2959.895	36899.516	465.200	995.312
58	5100.0	4.73460	156.869	3876.527	2774.141	34125.375	512.034	994.483
57	5000.0	4.78983	152.621	3723.905	2595.240	31530.135	559.390	993.925
56	4900.0	4.84422	148.325	3575.581	2423.294	29106.841	607.272	993.687
55	4800.0	4.89783	143.989	3431.592	2258.383	26848.458	655.688	993.821
64	4700.0	4.95073	130.023	3291.969	2100.552	24747.907	704.651	994.386
53	4600.0	5.00299	135.234	3156.734	1949.779	22798.128	754.177	995.445
52	4500.0	5.05469	130.833	3025.901	1806.076	20992.051	804.289	997.068
51	4400.0	5.10590	126.426	2899.475	1669.385	19322.667	855.012	999.330
50	4300.0	5.15669	122.021	2777.455	1539.631	17783.035	906.379	1002.317
49	4200.0	5.20713	117.625	2659.830	1416.725	16366.310	958.429	1006.122
48	4100.0	5.25729	113.243	2546.587	1300.533	15065.777	1011.207	1010.848

Level	Radius	Density	Mass of shell	Mass Within Radius	Moment of Inertia	Moment within Radius	Pressure	Gravity
No.	km	g/cm ³	10 ²⁴ g	10 ²⁴ g	10 ⁴⁰ g.cm ²	10 ⁴⁰ g.cm ²	k bar	cm/sec ²
47	4000.0	5.30724	108.883	2437.704	1190.942	13874.835	1064.767	1016.614
46	3900.0	5.35706	104.551	2333.152	1087.797	12787.039	1119.172	1023.550
45	3800.0	5.40681	100.252	2232.900	990.939	11796.100	1174.494	1031.804
44	3700.0	5.45657	96.165	2136.734	901.775	10894.325	1230.814	1041.459
43	3630.0	5.49145	97.178	2039.557	870.342	10023.983	1270.565	1032.803
42	3630.0	5.49145	0.000	2039.557	0.000	10023.983	1270.565	1032.803
41	3600.0	5.50642	40.991	1998.565	357.133	9666.850	1287.573	1028.983
40	3500.0	5.55641	133.753	1864.812	1124.123	8542.727	1344.157	1015.767
39	3480.0	5.56645	26.206	1838.606	212.793	8329.934	1355.440	1013.037
38	3400.0	5.60987	103.008	1735.599	812.820	7517.114	1400.496	1001.813
37	3300.0	5.66415	124.609	1610.990	932.622	6584.492	1456.591	987.097
36	3200.0	5.71843	119.888	1491.103	844.543	5739.949	1512.369	971.634
35	3100.0	5.77270	115.074	1376.028	761.536	4978.413	1567.772	955.430
34	3000.0	5.82698	110.181	1265.847	683.611	4294.802	1622.740	938.499
33	2900.0	5.88126	105.224	1160.623	610.764	3684.038	1677.213	920.853
32	2800.0	5.93553	100.217	1060.406	542.954	3141.084	1731.131	902.508
31	2700.0	5.98981	95.175	965.230	480.106	2660.978	1784.433	883.483
30	2600.0	6.04409	90.114	875.116	422.134	2238.844	1837.060	863.802
29	2500.0	6.09837	85.047	790.069	368.916	1869.928	1888.951	843.490
28	2400.0	6.15264	79.991	710.079	320.318	1549.610	1940.047	822.582
27	2300.0	6.20692	74.959	635.120	276.181	1273.429	1990.291	801.116
26	2200.0	6.26120	69.966	565.154	236.328	1037.100	2039.628	779.142
25	2100.0	6.31547	65.027	500.126	200.573	836.527	2088.003	756.721
24	2000.0	6.36975	60.157	439.969	168.709	667.819	2135.368	733.934
23	1900.0	6.42403	55.371	384.598	140.521	527.298	2181.678	710.878
22	1800.0	6.47831	50.684	333.914	115.786	411.511	2226.896	687.677
21	1787.5	6.48509	6.011	327.903	12.893	398.618	2232.456	684.776
20	1700.0	6.52703	40.089	287.814	81.349	317.269	2270.939	664.522
19	1600.0	6.88649	42.168	245.646	76.653	240.617	2314.824	640.272
18	1500.0	7.03784	38.415	207.231	61.633	178.984	2358.655	614.564
17	1400.0	7.09459	34.270	172.961	48.130	130.854	2401.336	588.826
16	1300.0	7.15135	30.164	142.798	36.733	94.121	2442.566	563.807
15	1221.5	7.17442	20.910	121.888	22.193	71.928	2473.835	545.091
14	1221.5	9.17442	0.000	121.888	0.000	71.928	2473.835	545.091
13	1200.0	9.18575	6.107	115.781	5.969	65.959	2484.512	536.500
12	1100.0	9.23583	25.837	89.944	22.851	43.108	2532.405	496.000
11	1000.0	9.28155	21.805	68.139	16.087	27.021	2576.798	454.664
10	900.0	9.32293	18.064	50.076	0.919	16.102	2617.562	412.515
9	800.0	9.35994	14.629	35.447	7.086	9.016	2654.582	369.568
8	700.0	9.39260	11.519	23.928	4.351	4.665	2687.749	325.841
7	600.0	9.42091	8.747	15.181	2.488	2.176	2716.972	281.380
6	500.0	9.44486	6.332	8.850	1.294	0.882	2742.182	236.210
5	400.0	9.46446	4.287	4.563	0.591	0.291	2763.336	190.294
4	300.0	9.47970	2.625	1.938	0.222	0.069	2780.457	143.683
3	200.0	9.49059	1.360	0.578	0.061	0.009	2793.727	96.419
2	100.0	9.49712	0.505	0.073	0.009	0.000	2804.037	48.710
1	0.0	9.49821	0.073	0.000	0.000	0.000	2805.297	0.000

The earth has a mass of 5121.820×10^{24} g, a moment of inertia of 76126.841×10^{40} g.cm², an average density of 4.7284 g/cm³, a density of 9.49821 g/cm³ and the pressure of 2805.297 kbar at earth's center. Each reduced values of the earth's data from that of the current earth are due to the existence of the dark planet within the interior of the earth. The dark planet has a radius of 3700.375 km, a moment of inertia of 4159.559×10^{40} g.cm², an average density of 4.0161 g/cm³, and a mass of 852.380×10^{24} g about 1.33 times of Mars. The data of the new earth model compares with that of the current earth and the PREM as listed in Table 8.

Table 8. The data of the new earth model compared with the data of the current earth and the PREM.

Data of planet	Radius	Mass	Inertia of moment	Average density	Center density	Center pressure	Coefficient
Unit	km	10^{24} g	10^{40} g.cm ²	g/cm ³	g/cm ³	k bar	
PREM and current earth	6371.000	5974.200	80286.400	5.515	13.08848	3638.524	0.3309
Earth planet	6371.000	5121.820	76126.841	4.7284	9.49821	2805.297	0.3662
Dark planet	3700.375	852.380	4159.559	4.0161	7.96097	1115.272	0.3564

The density of the earth's center is 9.49821 g/cm³, which is much lower than 13.08848 g/cm³ of the PREM. Its pressure is 2805.297 kbar, which is also much lower than 3638.524 kbar of the PREM. The composition of the inner core is generally believed to be dominantly iron with a small amount of alloyed nickel. From the pressure-density Hugoniot data for Fe, the density of iron under 2805.297 kbar of pressure is about 12.7 g/cm³ [Ahrens, 1980], which is much greater than that of the new earth model by about 25 %. The inner core is not pure iron but contains a significant fraction of light components [Ringwood, 1984; Jephcoat & Olson, 1987], and that explains why the density of the inner core is so much smaller than the current value. So, we may agree the composition of the inner core is dominantly iron, alloyed with a small amount of nickel and also combined with a significant number of oxides.

V. Acknowledgements

I am grateful to Dr. Lin-Gun Liu of Research School of Earth Science in Australian and Dr. Hsueh-Wen Yeh of Hawaii Institute of Geophysics for constructive criticisms and helpful comments.

VI. Discussion

Based on the results of this study, we infer that the solid rock in the lower mantle and the liquid molten rock or magma in the outer core change states interactively, and the density distribution are continuous at

the CMB. A great amount of the produced heat due to chemical reaction in the F zone and solidification at the ICB and the CMB become the geodynamo of a great convection cell, a circulation of magma and solid or molten rock migrating up to the crust and down to the F zone of the outer core and causes the topography of the core. The study introduces a new earth model which should solve many inexplicable problems of the earth, such as the density jump at the CMB, the core-mantle chemical equilibrium, the thermodynamic equilibrium of the inner and outer core, the geomagnetic secular variation and the Chandler wobble. Some improvements and refinements of the new earth model can be accomplished with the existing data. The anomalous properties of the CMB and the ICB are new sources of information that should impose important constraints on the short-term and long-term dynamic behavior of the core.

The fine structure of the CMB is not well known, but it contains information important to the geodynamic processes in the mantle or in the magnetic field generated in the outer core [Dziewonski & Woodhouse, 1987]. Approaching the Problem of the CMB, Creager and Jordan studied travel-time anomalies of PKiKP and PKP_{AB} and corrected for the mantle structure onto a region in the vicinity of the CMB [Creager & Jordan 1986]. They considered three hypotheses about the source of anomalies:

(1) the thin, heterogeneous D" region above the CMB, (2) perturbations in the CMB topography, and (3) a thin, highly heterogeneous layer below the CMB. Researchers agree that (2) is inconsistent with the data. Their data cannot distinguish between (2) and (3), and a reason for rejection of (2) is that core topography in excess of 10 km is considered unlikely. Morelli and Dziewonski reported that (3) should be rejected as the cause of the travel-time anomalies entering the core [Morelli and Dziewonski 1987]. But based on the great convection cell, which is the flowing matter migrating up to the crust and down to the F zone, a relief of the core in excess of 10 km in (2) provided by the three-dimensional maps should be accepted, and the secular variation of magnetic fields are from the flowing fluid due to the tangentially geostrophic and toroidal flows in the F zone.

From the simplification method, the new earth model, and the mass, density and radius of the dark planet, can be mathematically determined, with the results serving as an indirect proof of the existence of dark matter which locates in another cosmos of the universe. The dark planet inside the earth cannot be detected directly. If the Chandler wobble is analyzed in detail, it may be figured out. A more precise method of calculation can be used to figure out the data of the new earth model, but the differences of data between the precise and the approximate would be $\leq |10^{-3}|$, adopted from the data of Table 2.

Superstring theory has the positive figures of its fabulously largest of symmetries and miraculous cancellations of all the potential anomalies and divergences in quantum field theory. It provides a unifying description of elementary particles and forces of nature. But it has been pointed out by critics that the model has shortcomings and potential theoretical problems [Kaku, 1988] as follows:

1. It is impossible experimentally to reach the tremendous energies found at the scale of this theory.
2. The theory predicts that the energy scale is from 100 GeV over the next 17 orders of magnitude, which is unheard of in the history of science.
3. The theory does not explain why the cosmological constant is zero.
4. It is hard to select the correct way from apparently thousands of ways to break down the theory to low vacuum energies.

5. No one really knows how to break a ten-dimensional theory down to four dimensions. Of these five objections to the model, the most fundamental is the last — the inability to calculate dimensional breaking. This is why the search for the geometry underlying the theory is so important. The geometric formulation of the model may give us the key insight into the model that will allow us to make definite predictions with the theory. After studying the existence of the dark planet in the earth's interior, we should be able to confirm the three-cosmic structure in the universe. If the mathematicians and physicists take the geometric framework of ten-dimensional space-time in three cosmoses of the universe as a new way to explore Superstring theory, they should complete it successfully in a brief period of time.

From the application of the ten-dimensional space-time and the Supersymmetry of Superstring theory, we infer that the structure of the universe has three cosmoses, but that still needs to be proved by the outcomes of physicists' research. To demonstrate the three-cosmic structure of the universe from the existence of the missing neutrinos, we can plan a project of investigating anti-neutrino to observe another kind of neutrino which is emitted from nuclear plants.

References

- Altshuler, L. V. and Sharipdzhanov, L. V., 1971; **On the distribution of iron in the Earth and the chemical distribution of the latter.** *Bull. Acad. Sci. USSR, Geophys. Ser.*, **4**: 3-16.
- Ahrens, T. J., 1980; **Dynamic Compression of Earth Materials.** *Science* **207**: 1035. Birch, F., 1952; **Elasticity and constitution of the earth's interior.** *J. Geophys. Res.*, **57**: 227.
- Bloxham, J. and Gubbins, D. 1987; **Thermal core-mantle interactions.** *Nature*, **325**: 511-513.
- Bloxham, J. and Jackson, A., 1990; **Lateral temperature variations at the core- mantle boundary deduced from the magnetic field.** *Phys. Rev. Lett.*, Vol. 17, No. 11, 1997-2000.
- Blumenthal, G. R., Faber, S. M., Primack, J. R. and Rees, M. J., 1984; **Formation of galaxies and large-scale structure with cold dark matter.** *Nature*, **311**: 517-525.
- Bolt, B. A., 1972; **The Chemistry of the Earth's Core from Seismological Evidence.** *EOS.*, Vol. 53, No. 5, 599.
- Bolt, B. A. and Qamar, A., 1970; **Upper bound to the density jump at the boundary of the earth's inner core.** *Nature*, **228**: 148-150.
- Buchbinder, G. G., 1968; **Properties of the Core-Mantle Boundary and Observations of PcP.** *J. Geophys. Res.*, **73**: 5901.
- Buchbinder, G. G., Wright, C. and Poupinet, G., 1973; **Observations of PKiKP at distances less than 110.** *Bull. Seismol. Soc. Am.*, **63**: 1699-1707.
- Bullen, K. E., 1940; **The problem of the earth's density variation.** *Bull. Seismol. Soc. Am.*, **30**: 235-250.
- Chandler, S., 1891; **On the variation of latitude.** *Astronomical Journal*, **11**: 83.
- Cormier, V. F., 1981; **Short-period PKP phases and an elastic mechanism of thinner core.** *Phys. Earth Planet. Inter.*, **24**: 291-301.
- Creager, K. C. and Jorden, T. H., 1986; **A spherical structure of the core-mantle boundary from PKP travel time.** *Geophys. Res. Lett.*, **13**: 1497-1500.

- Derr, J. S., 1969; **Internal Structure of the Earth Inferred from Free Oscillations.** *J. Geophys. Res.*, **74**: 5202.
- Dziewonski, A. M. and Anderson, D. L., 1981; **Preliminary Reference Earth Model.** *Phys. Earth Planet. Inter.*, **25**: 297.
- Dziewonski, A. M. and Woodhouse, J. H., 1987; **Global Images of the Earth's Interior.** *Science*, **236**: 37-48.
- Engdahl, E. R., Flinn, E. A. and Romney, C. F., 1970; **Seismic waves reflected from the Earth's inner core.** *Nature*, **228**: 852-853.
- Engdahl, E. R., Flinn, E. A. and Masse, P., 1974; **Differential PKiKP travel times and the radius of the inner core.** *Geophys. J. R. astr. Soc.*, **39**: 457-463.
- Garland, G. D., 1979; **Introduction to Geophysics.** 2nd ED., W. B. Saunders Company, Toronto, Canada. 4-8, 28-30, 44-46, 130, 387-389.
- Gubbins, D. and Richards, M. A., 1986; **Coupling of the core dynamo and mantle: Thermal or Topography?** *Physical Review Letters*, **13**: 1521-1524.
- Gundmundsson, O., Clayton, R. W. and Anderson, D. L., 1986; **CMB topography inferred from ISC PcP travel times.** *Eos, Trans. AGU*, **67**: 1100.
- Hall, N., 1991; **May the forces be unified with Supersymmetry.** *New Scientist*, 6 April 11.
- Hall, T. H. and Murthy, V. R., 1972; **Comments on the Chemical Structure of an Fe-Ni-S Core of the Earth.** *EOS*, Vol. 53, No. 5, 602.
- Jeanloz, R., 1990; **The nature of the earth's core.** *Annu. Rev. Earth Planet. Sci.*, **18**: 357-386.
- Jeanloz, R. and Ahrens, T. J., 1980; **Equations of FeO and CaO.** *Geophys. J. R. Astr. Soc.*, **62**: 505-528.
- Jeanloz, R. and Wenk, H. R., 1988; **Convection and anisotropy of the inner core.** *Geophys. res. Lett.*, **15**: 72-75.
- Jephcoat, A. and Olson, P., 1987; **Is the Inner Core of the Earth Pure Iron?** *Nature*, **325**: 332-335.
- Kaku, M., 1988; **Introduction to Superstrings.** Springer Verlag New York Inc., New York, USA. 16-18.
- Knopoff, Leon, 1965; **a preeminent seismology,** *Phys. Rev.*, **138**: A 1445.
- Lay, T., 1989; **Structure of the Core-Mantle Transition Zone: A Chemical and Thermal Boundary Layer.** *Eos*, Vol. 70, No. 4, Jan. 24, 49, 54-55, 58-59.
- Lial, J. A. and Cormier, V. F., 1980; **Seismic waves at the Epicenter's antipodes.** *J. geophys. Res.*, **91**: 10203-10228.
- Lyttleton, R. A., 1973; **The end of the iron-core age.** *Moon*, **7**: 422-439.
- Lubin, P. M., Bond, J. R., Efstathiou, G. and Meinhold, P. R., 1991; **Cosmic-Structure Constraints from a One-Degree Microwave-Back-ground Anisotropy Experiment.** *Physical Review Letters*, **66**: 2179-2182.
- McQueen, R. G., Marsh, S. P., Taylor, J. W., Fritz, J. N. and Carter, W. J., 1970; **The equation of state of solids from shock wave studies, in high velocity impact phenomena.** Kinslow, R., Academic Press, New York, 294-419.
- Morelli, A. and Dziewonski, M., 1987; **Topography of the core-mantle boundary and lateral homogeneity**

- of the liquid core. *Nature*, **325**: 678-683.
- Ramsey, W. H., 1948; **On the constitution of the terrestrial planets.** *Mon. Not. Roy. Astron. Soc.*, **108**: 406-413.
- Ringwood, A. E., 1977; **Composition of the Core and Implications for Origin of the Earth.** *EOS.*, Vol. 58, No. 6, 519.
- Ringwood, A. E., 1984; **The Earth's Core: its composition, formation and bearing upon the origin of the Earth.** *Proc. R. Soc. A*, **395**: 1-46.
- Ruff, L. and Anderson, D. L., 1980; **Core formation, evolution, and convection: A geophysical model.** *Phys. Earth Planet. Inter.*, **21**: 181-201.
- Shearer, P. and Masters, G., 1990; **The density and shear velocity contrast at the inner core boundary.** *Geophys. J. Int.*, **102**: 491-498.
- Solomon, S. C., 1972; **Seismic-wave attenuation and partial melting in the upper mantle of North America.** *J. Geophys. Res.* **77**: 1483-1502.
- Souriau, A. and Souriau, M., 1989; **Ellipticity and density at the inner core boundary from subcritical PKiKP and PcP data.** *Geophys. J. Int.*, **98**: 39-54.
- Stevenson, D. J., 1987; **Limits on lateral density and velocity variations in the Earth's outer core.** *Geophys. J. R. astr. Soc.*, **88**: 311-319.
- Woodhouse, J. H. and Dziewonski, A. M., 1989; **Seismic modelling of the earth's large-scale three-dimensional structure.** *Phil. Trans. R. Soc. Lond. A* **328**: 291-308.
- Young, C. J. and Lay, T., 1987; **The core-mantle boundary.** *Ann. Rev. Earth Planet. Sci.*, **15**: 25-46.

The Certificate of Excellent Paper

